12th_Paper_Nurhasni_Hasan_(2019).pdf

by

Submission date: 04-Apr-2023 03:37PM (UTC+0700)
Submission ID: 2055485693
File name: 12th_Paper_Nurhasni_Hasan_(2019).pdf (1.87M)
Word count: 8770
Character count: 47657

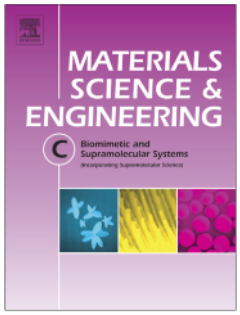

PEI/NONOates-doped PLGA nanoparticles for eradicating methicillin-resistant Staphylococcus aureus biofilm in diabetic wounds via binding to the biofilm matrix

Nurhasni Hasan, Jiafu Cao, Juho Lee, Muhammad Naeem, Shwe Phyu Hlaing, Jihyun Kim, Yunjin Jung, Bok-Leul Lee, Jin-Wook Yoo

PII: S0928-4931(18)33700-7
DOI: https://doi.org/10.1016/j.msec.2019.109741
Article Number: 109741
Reference: MSC 109741

To appear in: *Materials Science & Engineering C*

Received date: 3 December 2018
Revised date: 9 May 2019
Accepted date: 11 May 2019

Please cite this article as: N. Hasan, J. Cao, J. Lee, et al., PEI/NONOates-doped PLGA nanoparticles for eradicating methicillin-resistant Staphylococcus aureus biofilm in diabetic wounds via binding to the biofilm matrix, Materials Science & Engineering C, https://doi.org/10.1016/j.msec.2019.109741

PEI/NONOates-doped PLGA nanoparticles for eradicating methicillin-resistant *Staphylococcus aureus* biofilm in diabetic wounds via binding to the biofilm matrix

Nurhasni Hasan[a], Jiafu Cao[a], Juho Lee[a], Muhammad Naeem[a], Shwe Phyu Hlaing[a], Jihyun Kim[a,b], Yunjin Jung[a], Bok-Leul Lee[a], Jin-Wook Yoo[a*]

[a]Department of Manufacturing Pharmacy, College of Pharmacy, Pusan National University, Busan 46241, South Korea

[b]Department of Cogno-Mechatronics Engineering, College of Nanoscience & Nanotechnology, Pusan National University, Busan 46241, South Korea

*Correspondence: Jin-Wook Yoo, College of Pharmacy, Pusan National University, Busan 609-735, South Korea.

Tel: +82-51-510-2807; Fax: +82-51-513-6754; Email: jinwook@pusan.ac.kr

Abstract

Wounds infected with methicillin-resistant *Staphylococcus aureus* (MRSA) biofilm represent a high risk in patients with diabetes. Nitric oxide (NO) has shown promise in dispersing biofilm and wound healing. For an effective treatment of MRSA biofilm-infected wounds, however, NO needs to be supplied to the biofilm matrix in a sustainable manner due to a short half-life and limited diffusion distance of NO. In this study, polyethylenimine/diazeniumdiolate (PEI/NONOate)-doped PLGA nanoparticles (PLGA-PEI/NO NPs) with an ability to bind to the biofilm matrix are developed to facilitate the NO delivery to MRSA biofilm-infected wound. In simulated wound fluid, PLGA-PEI/NO NPs show an extended NO release over 4 days. PLGA-PEI/NO NPs firmly bind to the MRSA biofilm matrix, resulting in a greatly enhanced anti-biofilm activity. Moreover, PLGA-PEI/NO NPs accelerate healing of MRSA biofilm-infected wounds in diabetic mice along with complete biofilm dispersal and reduced bacterial burden. These results suggest that the biofilm-binding NO-releasing NPs represent a promising NO delivery system for the treatments of biofilm-infected chronic wounds.

Keywords

Nitric oxide releasing nanoparticles; Methicillin-resistant *Staphylococcus aureus*; Diabetic wounds; Anti-biofilm; Wound healing

1. Introduction

Biofilms are surface-attached bacterial communities embedded in a hydrated extracellular polymeric substance (EPS) mostly composed of exopolysaccharides and proteins [1, 2]. The wounded skin provides a favorable environment for bacterial colonization and biofilm formation due to sufficient nutrients and a suitable surface for biofilm attachment [3]. Biofilm infections in wounds can cause delayed wound healing, tissue necrosis, and systemic infection and can be associated with cross-contamination between hospitalized patients (i.e. nosocomial infections) [1, 4, 5]. The Gram-positive *Staphylococcus aureus* is the most common bacterium in biofilm-associated chronic wound infections [6, 7]. Importantly, methicillin-resistant *Staphylococcus aureus* (MRSA) is largely associated with biofilms in cutaneous wounds and responsible for significant morbidity and mortality worldwide [8-11]. In particular, MRSA biofilm-caused wound infections pose a high risk in diabetic patients who lack crucial factors needed for an effective immune response against pathogens [12, 13]. For example, chronic diabetic foot ulcers associated with MRSA biofilms often result in lower-limb amputations [14]. Because of the high prevalence of MRSA biofilms in wounds, there is an urgent need for effective therapies to treat MRSA biofilm-infected wounds.

An effective medication for the treatment of biofilm-infected wounds need to disperse the biofilm, eradicate planktonic bacteria, and stimulate proliferation and tissue remodeling. However, current options for treating MRSA biofilm-infected wounds include antibiotics and anti-biofilm agents such as silver and ethylendiaminetetraacetic acid (EDTA), both of which do not promote tissue proliferation and remodeling [15, 16]. Moreover, it has been observed that they delay wound healing and may have cytotoxic side effects [17]. Furthermore, there is a growing concern about the emergence of antibiotic-resistant infections [18, 19]. Therefore, there is an urgent need for new treatments of biofilm-infected wounds.

In recent years, NO has emerged as a potent anti-biofilm, antibacterial, and wound-healing agent [20-23]. NO regulates the intracellular secondary messenger cyclic di-GMP, which stimulates effectors that prevent biofilm formation and disperse established biofilms [24]. In particular, reactive nitrogen species derived from NO and superoxide ($O_2^{\bullet-}$) act by downregulating the production of polysaccharide intercellular adhesin, which is crucial for developing a strong substrate attachment by MRSA cells [25]. Moreover, NO kills MRSA by causing cell wall damage and lysis [26]. NO also accelerates wound healing by stimulating cell proliferation, wound contraction and collagen remodeling [27]. However, clinical application of NO is hampered by its gaseous properties and a short half-life (2-3 sec).

Various NO delivery systems such as sol-gel, films, hydrogels, microparticles, dendrimers, and micelles have been tested for controlled release of NO, a prerequisite for overcoming the limitation of its gaseous properties [28-34]. Interestingly, NO-releasing nanoparticles (NPs) have gained much attention because of their high surface-area-to-volume ratio, which creates chemical flexibilities and beneficial physical properties, and a small size, which enables efficient interaction with micron-size bacteria [35-40]. However, quick degradation of NO upon release restricts its diffusion distance to approximately 150-300 μm, resulting in limited utilization of NO delivery systems including NO-releasing NPs. Thus, unless NO-releasing NPs are in proximity to the target, substantial reduction of NO activity can occur.

To address the challenge, we developed NO-releasing NPs with an ability to directly bind to the biofilm matrix that provide enhanced NO availability in biofilm-infected wound areas, thereby enabling an effective treatment of the wounds. We used poly(lactic-*co*-glycolic acid) (PLGA) as NP-forming polymer and polyethylenimine/diazeniumdiolate (PEI/NONOate) as a NO donor and a biofilm-binding polymer to synthesize PEI/NONOates-doped PLGA NPS (PLGA-PEI/NO NPs). The particle size, polydispersity index, and NO loading capacity of PLGA-PEI/NO NPs were characterized. A NO release profile of PLGA-PEI/NO NPs was evaluated in simulated wound fluid (SWF). After physicochemical characterization, *ex vivo* biofilm-binding capability and *in vitro* and *in vivo* anti-biofilm activity of PLGA-PEI/NO NPs were investigated. *In vivo* wound-healing activity and wound bacterial burden were evaluated in diabetic mice with MRSA biofilm-infected wounds.

2. Materials and Methods

2.1. Materials

NO and nitrogen (N_2) gasses were obtained from Hana Gas Inc. (Gimhae, Korea). PLGA (50:50 DLG 5E) was purchased from Lakeshore Biomaterials (Birmingham, AL, USA). Linear PEI (MW 25 kDa), sodium methoxide ($NaOCH_3$), crystal violet, 3-(2-benzothiazolyl)-7-(diethylamino)coumarin (coumarin-6), STZ, tetramethylrhodamine isothiocyanate (TRITC), Mayer's hematoxylin, eosin-Y disodium salt, bovine serum albumin (BSA), Tetrazolium dye 3-(4,5-di-methylthiazol-2-yl)-2,5 diphenyltetrazolium bromide (MTT), dimethylsulfoxide (DMSO) and Griess assay reagent were purchased from Sigma-Aldrich (St. Louis, MO, USA). Bacto™ tryptic soy broth (TSB) medium was procured from BD Biosciences (Sparks, MD, USA). Masson's trichrome stain (connective tissue stain) was

purchased from Abcam (Cambridge, MA, USA). Tiletamine/Zolazepam (Zoletil 50®) was obtained from Virbac S.A. (Virbac, Carros, France) and xylazine hydrochloride (Rompun®) was obtained from Bayer (Leverkusen, Germany). Polyurethane coupon (high-temperature polymer) was purchased from Biosurface technologies corporation (Bozeman, MT, USA). The LIVE/DEAD® Baclight™ bacterial viability kit (Molecular Probes) was purchased from Life Technologies (Eugene, Oregon, USA). The Roswell Park Memorial Institute (RPMI) 1640 medium, trypsin, fetal bovine serum (FBS), and penicillin-streptomycin were purchased from Hyclone, Thermo Fisher Scientific Inc. (Waltham, MA, USA). All other reagents and solvents used were of the highest analytical grade.

2.2. NP preparation

An oil-in-water emulsification solvent evaporation method was used with slight modifications to synthesize PLGA NPs, PLGA-PEI NPs and PLGA-PEI/NO NPs [41-43]. Briefly, PLGA (140 mg) was mixed with either PEI or PEI/NONOate (60 mg), dissolved in DCM (8 mL) and poured into a solution of cold poly(vinyl alcohol) (PVA, 1%, 20 mL). For fluorescence labeling, coumarin-6 (0.5 mg) was added to the polymer solution. The solution was stirred using a high-speed homogenizer (IKA®T10 ULTRA-TURRAX ®, Germany) at 14,500 rpm for 2 min in an ice bath, followed by probe sonication (KFS-300N Ultrasonic, Korea) at 150 W in an ice bath for 3 min. The emulsion was then added to NaOH (10 mL, 0.0001 M) and stirred at 4 °C for 8 h. After the residual solvent was removed, the emulsion was centrifuged at 20,000 × g at 4 °C for 30 min and washed two times with alkaline solution pH 8. The pellets were freeze-dried and stored at -20 °C up to one month before usage.

2.3. Characterization of NPs

The morphological characteristics of NPs were recorded using a field emission electron microscope with EBSD system (FE-SEM, Supra 40VP, Carl Zeiss AG, Germany). The particle size and polydispersity index (PDI) were measured using a Zetasizer Nano series ZS90 (Malvern Instruments, Herrenberg, Germany) and qNano size analyzer (iZON Sciences, Christchurch, New Zealand). For the zeta potential measurement, Zetasizer nano ZS90 was used. The NP particle size distribution was described using the cumulant mean (z-average) ± standard deviation (SD) and the PDI.

2.4. *In vitro* NO release

The release of NO from PLGA-PEI/NO NPs was evaluated in SWF at 37 °C. PLGA-PEI/NO NPs (1 mg) was added to the SWF pH 7.1 (1 mL) and incubated at 37 °C with mild stirring. At predetermined time intervals, samples were centrifuged at 20,000 × *g* and 4 °C for 15 min. The supernatant was further diluted and 100 μL were withdrawn and mixed with Griess reagent (100 μL) before incubation for 15 min at 25 °C in the dark. The absorbance was measured at 540 nm using a Biorad iMark™ microplate reader (Bio-Rad Laboratories, Inc. USA). The amount of NO released from PLGA-PEI/NO NPs was calculated using sodium nitrite ($NaNO_2$, 0–100 μM) as a standard.

2.5. *Ex vivo* biofilm binding of NPs

The MRSA biofilm samples were obtained from mice to evaluate the adhesion of the NPs to the biofilm, followed by fixation in a glutaraldehyde solution (5%) for 1 h. Biofilm were immersed in PBS containing coumarin-6 labeled NPs (5 mg/mL) and incubated for 2 h at 37 °C with mild shaking. Biofilms were washed three times with NaCl (0.85%) to remove the unbound NPs and added TRITC dye. The samples were then incubated with shaking for 5 min and another 1 h without shaking at 25 °C in dark place. Biofilms were washed twice with NaCl (0.85%) and then removed from rinse solution and transferred onto the slides. The adhesion of NPs on biofilm was observed with a confocal microscope at ex/em wavelengths of 490/520 nm for FITC (labeled NPs) and 557/576 nm for TRITC (labeled biofilm).

2.6. In vitro anti-biofilm activity

MRSA USA300 FPR3757 (GenBank accession no. NC_00793) was used for testing anti-biofilm activity. Bacterial suspension (10^7 CFU/mL, 100 µL) was placed on the surface of a polyurethane coupon and incubated at 37 °C for 8 h. Then, TSB medium (1.7 mL) along with the PLGA-PEI/NO NPs (200 μL) were added at final NP concentrations of (2.5, 5, and 10 mg/mL) in 12-well plates. Phosphate-buffered saline (PBS; pH 7.4) was used as a control. All samples were incubated at 37 °C for 8, 12, and 24 h. After incubation, biofilm on the coupons was washed twice with PBS and crystal violet solution (1 mL, 0.1%) was added. The coupons were incubated for 20 min and washed again with PBS. The amount of remaining crystal violet biofilm was quantified by measuring OD_{550} after adding ethanol (1 mL, 100%). For a confocal microscopy study, the bacterial suspensions (after biofilm dispersal) were stained with LIVE/DEAD® Baclight™ bacterial viability kit reagents according to the manufacturer's protocol. The samples were analyzed with an FV10i Fluoview confocal

microscope to differentiate between live and dead bacteria. Bacteria stained green with Syto-9 at the excitation (ex)/emission (em) wavelengths of 539/570–620 nm were considered viable/live and that stained red with propidium iodide (PI) at ex/em 470/490–540 nm were considered dead.

2.7. STZ-induced diabetic mice

Mice were fasted for 4 h prior to intraperitoneal (i.p.) injection of STZ, a β-cell cytotoxic agent that induces type 1 diabetes mellitus [44]. Balb/c and ICR received a single dose of STZ at (200 mg/kg) freshly dissolved in sodium citrate buffer (0.05 M), pH 4.5. Hyperglycemia was confirmed by measuring the fasting blood glucose level one month post-injection. Mice with fasting blood glucose levels above (300 mg/dL) were considered to be diabetic.

2.8. Formation and characterization of *in vivo* MRSA biofilm in wound

The bacteria were grown in TSB medium overnight at 37 °C with agitation at 100 rpm and diluted for growth until the mid-exponential phase. Bacterial suspension (60 µL) with a final concentration of 10^7 CFU/mL was placed on the surface of the skin wound and lightly scrubbed with sterile Teflon spatula before being covered with a membrane filter that was dipped into bacteria suspension. The infected wound was covered with a polyurethane film dressing (Tegaderm Transparent Dressing; 3M Health Care, St. Paul, MN) for 48 h to provide a suitable environment for colonization.

Incisional biopsies were investigated to evaluate the biofilm formation in the wound. Briefly, one diagonal section approximately 3 mm thick was recovered from the central part of the wound and fixed in a glutaraldehyde solution (5%) for 1 h. Then the biopsies were rinsed twice in PBS. For electron microscopy, the biopsies were placed on carbon tape and vacuum-dried overnight before coating with gold for 2 min under vacuum. The samples were then viewed with the Hitachi S3500N SEM (Hitachi, Japan) at an accelerating voltage of 15 kV. For confocal microscopy, the fixed samples were washed in NaCl (2 ml, 0.85%) and added SYTO-9 (ex/em; 539/570-620 nm) and TRITC dye (ex/em; 557/576). The samples were incubated with shaking for 5 min and another 1 h without shaking at 25 °C in the dark. Cells were washed once with PBS and twice with NaCl (0.85%). Samples were removed from NaCl (0.85%) rinse solution and transferred onto slides. Biofilms or adhered cells were observed with the FV10i Fluoview confocal microscope to confirm EPS labeling with red

color and bacteria labeling with green color. In preparation for Gram staining, the incisional biopsies from wound day 7 (untreated group) were fixed with formaldehyde (10%) and blocked with paraffin. Five-micron vertical sections were fixed to glass slides and stained by Gram staining to observe MRSA colonies in the wound. The slides were examined using light microscopy (Olympus BX53) and images were digitally captured at a resolution of 1360 × 1024 pixels using an Olympus DP70 digital camera.

2.9. *In vitro* cytotoxicity study

L929 mouse fibroblasts from the Korean Cell Line Bank (KCLB, Seoul, Korea) were cultured in RPMI medium supplemented with 10% (v/v) FBS and antibiotics (100 IU/mL penicillin G sodium and 100 μg/mL streptomycin sulfates). The cells were overnight incubated in an incubator supplied with 5% CO_2 and a humidified air atmosphere at 37 °C and then were seeded on a 96-well plate at 2.5×10^4 cells per well. After 48 h, the media were then replaced with fresh media containing PLGA NPs, PPNPs, and PLGA-PEI NPs at various concentrations (2.5, 5, and 10 mg/mL). After 24 h of incubation, a standard MTT solution in sterile PBS was added to each well and cells were incubated for 2 h. The MTT solution was then removed and 150 μL of DMSO was added to each well. The absorbance measured at 540 nm was proportional to the concentration of viable cells in each well. Untreated cells were used as a control. The data were expressed as mean ± standard deviation of eight replicates (n=8). The cell viability was calculated using the following equation:

$$\textbf{Cell viability}\ (\%) = \frac{\boldsymbol{Absorbance\ (treated\ cells)}}{\boldsymbol{Absorbance\ (control\ cells)}} \times \mathbf{100}$$

2.10. *In vivo* wound healing activity

All animal experiments were performed in accordance with the regulations of Pusan National University and Korean Legislation on animal studies. Male ICR and BALB/c mice (7–8 weeks, Samtako Bio Korea) were used. The mice were anesthetized by i.p. injection using Zoletil®50 and Rompun® at a ratio of 5:2 prior to the development of wounds in the dorsal area. The dorsal hair was shaved with an electric razor and the back skin was excised with an 8-mm biopsy punch to create full-thickness wounds. The wound infection models were divided into 2 categories, biofilm-challenged in STZ-induced diabetic ICR mice and Balb/c mice (see Supporting information) and non-diabetic (ICR and Balb/c mice, see supporting information). Biofilm-infected wounds were obtained by treating the wound as

described in section "formation and characterization of *in vivo* MRSA biofilm in wound". Ten milligram of the freeze-dried PLGA-PEI NPs and PLGA-PEI/NO NPs were topically applied from day 2 post-injury. Each wound was covered with sterile gauze. Untreated mice were used as a control. The gauze on the wound lesions was replaced with new gauze at the proper time. Photographs of the wounds were taken to observe the gross visual wound healing as determined by the wound area not covered by the migrating epithelial cells. The ImageJ software (National Institutes of Health, Bethesda, Maryland) was used to determine the wound size reduction, which was calculated as follows:

$$\text{Wound size reduction (\%)} = \frac{Wt}{Wo} \times 100$$

Where, W_0 is the wound area at start time 0 and W_t is the wound area at time t.

2.11. Histological processing

The cross-sectional full-thickness skin specimens and deep granulation tissues were collected on the last day of the *in vivo* experiment. Full wound areas were excised, fixed in formaldehyde (10%) for 24 h and blocked with paraffin. Five-micron vertical sections were fixed to glass slides and processed with Gram stain, Hematoxylin and eosin (H&E) stain, and Masson's trichrome stain to evaluate bacteria, skin morphology, and collagen formation, respectively. The slides were analyzed by light microscopy (Olympus BX53) and images were digitally captured at a resolution of 1360 × 1024 pixels with an Olympus DP70 digital camera.

2.12. Reduction of wound bacterial burden

The bacterial burden (bacterial viability) in the wound was examined 12-14 days post-injury in both non-diabetic and diabetic group mice. At day 2 post-injury and MRSA inoculation, a sterile swab with PBS was applied superficially to the biofilm-infected wound and plated on TSB agar for a superficial examination. After examination of the wounds at day 8, and 12 (post-inoculation), wound skin tissues were recovered, homogenized, and diluted in sterile PBS. Each dilution (200 µL) was plated on TSB agar medium and incubated at 37 °C overnight. The colonies per plate were counted to determine the number of viable bacteria at the time of plating.

2.13. Fluorescence visualization of *in vivo* MRSA biofilm dispersal

We monitored *in vivo* MRSA biofilm dispersal by confocal microscopy, visualizing the EPS content change in the biofilm using a red stain, TRITC (ex/em wavelengths of 557/576 nm). The change in bacteria density inside the biofilm was also visualized using SYTO-9 (ex/em wavelengths of 539/570–620 nm). The *in vivo* MRSA biofilm of each observation day (day 0, 4, 6, 8, 10 post-treatment) was treated as described in section 2.7. Biofilms and bacteria were observed with the FV10i Fluoview confocal microscope. EPS were labeled with red, bacteria were labeled with green. Images were analyzed in side view.

2.14. Statistical analysis

Statistical analysis was performed using one-way analysis of variance (ANOVA) followed by Tukey's multiple comparison tests or using unpaired t-test in GraphPad Prism 5.0 (GraphPad Software, La Jolla, California). In cases of significant deviations from the t-test, the nonparametric Mann-Whitney U test was conducted to compare the distributions of two unpaired groups. A value of $P < 0.05$ was considered statistically significant. The data are presented as the mean ± SD.

3. Results and discussion

3.1. NP preparation and characterization

The goal of this study was to develop NO-releasing NPs that efficiently disperse biofilms, eradicate bacteria, and subsequently accelerate proliferation and remodeling of MRSA biofilm-infected wound tissues. The anti-biofilm/antibacterial and wound healing activities of NO have been well demonstrated in several studies; however, due to a short-half life (2–3 sec) and a limited diffusion distance (approximately 150–300 μm) of NO, delivery of sufficient amount of NO to biofilm-infected wounds remains a difficult task. Thus, in this study, we prepared PLGA-PEI/NO NPs with a prolonged NO release profile and biofilm-binding property. Upon binding to the matrix of MRSA biofilm, PLGA-PEI/NO NPs can continuously supply a sufficient amount of NO to the biofilm-infected wound area, leading to enhanced anti-biofilm, antibacterial, and wound healing activities.

In this study, nanoparticles (PLGA NPs, PLGA-PEI NPs, and PLGA-PEI/NO NPs) were prepared by an oil-in-water emulsification solvent evaporation method (**Fig. 1**). The physicochemical properties of NPs were characterized as shown in **Table 1**. The average size of PLGA NPs, PLGA-PEI NPs, and PLGA-PEI/NO NPs measured by the Zetasizer was 252

± 45 nm, 265 ± 11 nm, and 240 ± 2 nm, respectively. qNano results confirmed that there was no noticeable difference in particle size. The scanning electron microscopy (SEM) image of prepared NPs revealed a spherical morphology (**Fig. 2A**). The PDI values of PLGA NPs, PLGA-PEI NPs, and PLGA-PEI/NO NPs were 0.133, 0.091, and 0.080 respectively. The particle size distributions (**Fig. 2B**) and PDI values revealed a narrow size distribution. The zeta potential of PLGA NPs was a negative charge (-24.3 mV), whereas PLGA-PEI NPs and PLGA-PEI/NO NPs were positively charged with values of +34.5 and +34.6 mV, respectively. The amount of NO loading of PLGA-PEI/NO NPs was 122 ± 1 µmole/g NPs.

3.2. *In vitro* NO release

Following the successful preparation of nanoparticles, we investigated whether PLGA-PEI/NO NPs can release NO in a wound area for prolonged periods of time. The NO release study was performed in SWF that mimics *in vivo* wound conditions. Wound fluid consists of a variety of components ranging from basic electrolytes to proteins, which can affect the NO release from PLGA-PEI/NO NPs [45]. As shown in **Fig. 2C**, the NO release profile exhibited a biphasic pattern with a fast release in the first 24 h (~85%), followed by a sustained release of over 4 days. The drug-release mechanism from PLGA NPs followed the diffusion- and degradation-controlled release type [46]. The fast NO release in the first 24 h and the subsequent sustained NO release could be beneficial for disrupting the matrix of MRSA biofilms and subsequent antibacterial activity. It is worth to note that dispersal of biofilm requires a higher amount of NO than that for killing planktonic bacteria [47]. Furthermore, the sustained release of NO can also accelerate proliferation and remodeling of wound tissues [26, 48].

3.3. *Ex vivo* biofilm binding of NPs

The other key property of a NO-releasing system for treating biofilm-infected wounds is the ability to maintain a high NO concentration in the wound area, which can be achieved by binding to the biofilm matrix. Again, it should be noted that the site of action of NO needs to be close to a NO-releasing system because NO has a short diffusion distance (150–300 µm) [32]. Since exopolysaccharides in biofilms are highly anionic due to the presence of uronic acid (D-glucoronic acid, D-galacturonic and D-mannuronic acid), ketal-linked pyruvate, carboxyl, phosphate, and sulfate groups [49], we hypothesized that the cationic property of PLGA-PEI/NO NPs (+34.6 mV, **Table 1**) facilitates an electrostatic interaction between

cationic PLGA-PEI/NO NPs and the negatively charged biofilm matrix, thereby increasing NO availability in the biofilm-infected wound area. As shown in **Fig. 3**, the adhesion of NPs to the biofilm matrix was evaluated by confocal microscopy. In **Fig. 3A**, the red, green and yellow color represents TRITC-labeled biofilm matrix, coumarin-6-labeled NPs, and NPs bound to the biofilm matrix, respectively. Only a negligible amount of PLGA NPs was found on the biofilm matrix, whereas an abundant amount of PLGA-PEI NPs and PLGA-PEI/NO NPs was observed in the biofilm matrix, indicating the strong binding of positively charged NPs to the biofilm. **Fig. 3B** illustrates the hypothesis of NP binding to the biofilm matrix. It showed the repulsion of negatively charged NPs by the biofilm matrix with the same charge. Conversely, the positively charged NPs bind to the biofilm matrix, demonstrating that cationic NPs strongly interact with the negatively charged biofilm matrix.

3.4. *In vitro* anti-biofilm activity

Next we assessed the *in vitro* anti-biofilm activity of PLGA-PEI NPs and PLGA-PEI/NO NPs against MRSA biofilm using a crystal violet staining method on the polyurethane coupons. Crystal violet stains macromolecules including the biofilm matrix composed of EPS [50]. The *in vitro* anti-biofilm activities of PLGA-PEI NPs and PLGA-PEI/NO NPs at different NPs concentrations (2.5, 5 and 10 mg/mL) and incubation times (8, 12, and 24 h) are shown in **Fig. 4A** and **4B**. Purple color represents biofilm attachment to the polyurethane coupon. Blank NPs (PLGA-PEI NPs) did not cause detectable biofilm dispersal (**Fig. 4A**) or a reduction of biofilm biomass (**Fig. 4B**), whereas PLGA-PEI/NO NPs showed significant biofilm dispersal activity in a concentration- and time-dependent manner. At 2.5 mg/mL, biofilm dispersal was detected at the 12 h and 24 h incubation time. The reduction in biofilm mass measured at OD_{550} was 5.5% and 67% at 12 h and 24 h, respectively. The anti-biofilm activity was associated with PLGA-PEI/NO NPs concentration. At 5 and 10 mg/mL, the faded purple color was more prominent than concentration of 2.5 mg/mL, particularly at the 24 h incubation time that showed a coupon color almost similar to the control lacking a biofilm. The results were linked to the reductions in biofilm mass (**Fig. 4B**). At 5 mg/mL PLGA-PEI/NO NPs the biofilm mass reductions were 7.9%, 36%, and 73.1% after 8, 12, and 24 h incubation time, respectively. At 10 mg/mL, the reductions were 39.6%, 61.9%, and 94% at 8, 12, and 24 h incubation time, respectively. The red dot box on **Fig. 4A** showed confocal microscopy images of the planktonic bacteria after biofilm dispersal by 10 mg/mL PLGA-PEI/NO NPs treatment, demonstrating that PLGA-PEI/NO NPs not only disperse the biofilm

but kill the planktonic bacteria upon biofilm dispersal. The minimum inhibitory concentration (MIC) of PLGA-PEI/NO NPs against MRSA is 0.625 mg/mL.

3.5. Formation and characterization of *in vivo* MRSA biofilm in wound

Prior to the *in vivo* biofilm dispersal and wound healing studies, we first confirmed *in vivo* formation of MRSA biofilms on wound beds of diabetic mice because MRSA biofilm on diabetes-associated wounds has not been established elsewhere to our best knowledge. **Fig. S1A** showed that the wound surface was fully covered by the MRSA biofilms. The EPS matrix and the bacterial colony was found on the wound bed by SEM images (yellow arrow, **Fig. S1B**) and by Gram staining images (yellow arrow, **Fig. S1C**), respectively. As shown in **Fig. S1D**, 3D confocal images showed that the EPS matrix (red color) encloses bacterial micro colonies (green color), further confirming the formation of MRSA biofilms. The cross-sectional images of selected biofilm area showed the close-up view of the structural organization of bacteria (green) and EPS (red) during the development of mature biofilm (**Fig. S1E**), indicating that mature biofilms on the wound bed were successfully formed.

3.6. *In vitro* cytotoxicity study

We evaluated *in vitro* cytotoxicity of blank NPs (i.e. PLGA NPs and PLGA-PEI NPs) and PLGA-PEI/NO NPs on healthy mammalian fibroblast cells (L929). Mammalian fibroblast cells provide an excellent model due to their significant roles in wound healing and maintaining the extracellular matrix [51]. As shown in **Fig. 5**, the blank PLGA NPs, PLGA-PEI NPs, and PLGA-PEI/NO NPs groups showed cell viability over 80% in the NPs concentration up to 5 mg/mL, indicating no toxicity to mammalian fibroblast cells (L929). At a concentration of 10 mg/mL, NPs exhibited 76.2%, 69,1%, and 66.4% of cell viability for blank PLGA NPs, PLGA-PEI NPs, and PLGA-PEI/NO NPs, respectively. Since PLGA is known as an FDA-approved biodegradable and biocompatible polymer, the cytotoxicity of PLGA NPs might be due to the presence of a high number of particles used in *in vitro* cytotoxicity study. The viabilities of fibroblast cells treated with PLGA-PEI NPs and PLGA-PEI/NO NPs were not much different from those treated with blank PLGA NPs, revealing the cytotoxicity of the NPs at 10 mg/mL is caused mostly by the high number of particles and NO per se did not significantly affect the viability of fibroblast cells. It is worth to note that the circumstance of *in vitro* cytotoxicity study is quite different from that of *in vivo* MRSA biofilm-infected wounds. NPs used in *in vitro* cytotoxicity study contact directly on

fibroblasts cells during incubation, whereas under *in vivo* condition, NPs are applied on the biofilm surface and thus are not likely to physically interact with skin fibroblast cells, implying that *in vitro* cytotoxicity caused by a high number of particles can be ignored. Furthermore, H&E staining results obtained from *in vivo* wound tissues support that there is no sign of cytotoxicity with PLGA-PEI/NO NPs treatment. PLGA-PEI/NO NPs group did not show any sign of cytotoxicity such as the presence of foreign body and granuloma [52]. More importantly, fibroblast cells were fully recovered without noticeable reduction of fibroblast cells, demonstrating that *in vitro* cytotoxicity caused by a high number of blank NPs did not occur under *in vivo* circumstance (**supporting information, Fig. S2**).

Nevertheless, the toxicity of PLGA-PEI/NO NPs to L929 mammalian fibroblast cells is minimal as compared to commercially available topical antiseptics and other NO-releasing systems [33, 53-55]. Povidone iodine and chlorhexidine, both of which are well known topical antiseptics, substantially decreased cell viability of human fibroblast cells by approximately 89% and 100%, respectively [54, 55]. Despite the striking cytotoxicity, however, povidone iodine and chlorhexidine are still clinically available because they can effectively control infection and promote healing in bacteria-infected wounds [56]. Furthermore, several studies reported that NO-releasing systems are considered acceptable or tolerable when they are less toxic than those commercial antiseptics [53, 57-59]. Thus, the *in vitro* cytotoxicity of PLGA-PEI/NO NPs to L929 mammalian fibroblast cells would not be a significant drawback to their potential biofilm-infected wound therapy.

3.7. *In vivo* biofilm dispersal and wound healing activities

The *in vivo* biofilm dispersal and wound healing activities of PLGA-PEI/NO NPs were evaluated in MRSA biofilm-infected wounds in diabetic mice and non-diabetic mice. PLGA-PEI NPs without NO were used as a control. As shown in **Fig. 6A and S3A**, PLGA-PEI/NO NPs treatment dispersed the biofilm followed by accelerated wound healing in diabetic ICR mice and Balb/c mice, whereas untreated and blank NPs (PLGA-PEI NPs) did not affect the biofilm or the wound size. In PLGA-PEI/NO NPs treated groups, the *in vivo* MRSA biofilm dispersal was observed at day 8 post-injury in both diabetic mice model. Following the biofilm dispersal (from day 8 post-injury), the wound area of mice skin lesions relative to the initial 8-mm wound was also significantly reduced (**Fig. 6B and S3B**). The percentage of wound closure observed at last day (day 12 post-injury) was 92.2% ($P < 0.05$) in diabetic ICR mice and 95.5% ($P < 0.05$) in Balb/c mice (**Fig. 6C and S3C**). The occurrence of MRSA

biofilm infection may also happen in a non-diabetic condition, thus we also investigated the potency of our system for the treatment of MRSA biofilm-infected wound in non-diabetic ICR and Balb/c mice. The effects of PLGA-PEI/NO NPs on biofilm dispersal and wound healing in non-diabetic ICR and Balb/c mice were similar to the observations in diabetic condition (**Fig. S4**). The PLGA-PEI/NO NPs group showed nearly complete wound closure and re-epithelialization by the day 12 post-injury in all wound models. Interestingly, PLGA-PEI/NO NPs group showed *in vivo* biofilm dispersal followed by the fast wound closure from the day 8 post-injury. In contrast, the untreated and PLGA-PEI NPs group showed neither biofilm dispersal nor wound healing at all. The delayed wound healing in the untreated and PLGA-PEI NPs group particularly in diabetic model can be attributed to diabetic condition which is a well-known cause of chronic wounds [60].

3.8. Histological analyses

We also examined the progress of wound healing by histological examination of H&E staining and Masson's trichrome staining, which visualized the skin layer morphology and collagen deposition respectively. Unlike in the untreated and PLGA-PEI NPs groups, the PLGA-PEI/NO NP-treated mice group showed a skin morphology similar to normal skin in diabetic ICR and Balb/c mice model (**Fig. 7 and S3D**). The microscopic images of H&E and Masson's trichrome staining of untreated and PLGA-PEI NPs group showed open wound and early epithelialization, ulceration, and an abundance of mononuclear inflammatory cells with deep inflammatory infiltration passing through the dermal layer and a lack of collagen. By contrast, PLGA-PEI/NO NPs group showed increased numbers of fibroblast-like cells (**Fig. S2**) and collagen deposition along with decreased numbers of mononuclear inflammatory cells and healed skin structures close to normal healthy skin. The effect of NO in collagen formation would be mainly due to the deterrence of collagen degradation by MRSA in the infected tissue or the posttranslational escalation of collagen synthesis instead of *de novo* transcription of the pertinent collagen genes [26, 61]. The histological results in the non-diabetic group (**Fig. S4D**) did not differ from those in the diabetic group.

3.9. Reduction of wound bacterial burden

Finally, bacterial burden in the wound was evaluated by CFU counts to determine bacteria viability and by Gram staining to detect bacterial colonies in the wounded skin (**Fig. 8A and 8B**). As shown in **Fig. 8A**, the PLGA-PEI/NO NPs group have an approximately 2-

log reduction (~90% killing) in bacterial viability at day 8 post-injury in STZ-induced diabetic ICR mice and almost no bacterial load was detected at day 12 post-injury. The untreated and PLGA-PEI NPs group showed no significant change in bacterial viability; however, the number of bacteria that colonized the wound increased. In line with the result, the Gram staining images (**Fig. 8B**) of the tissue at day 12 showed intradermal infections on untreated and PLGA-PEI NPs groups as indicated by purple color. However, the PLGA-PEI/NO NPs group did not show bacterial skin infections, indicating that PLGA-PEI/NO NPs can completely eradicate the bacteria. *In vivo* biofilm dispersal was also visualized by a confocal microscope. As shown in **Fig. 8C,** the biofilm matrix (EPS stained in red by TRITC) gradually decreased from day 0 to day 10. It also showed that there was reduction in the number of bacteria colonized the inside of the biofilm matrix.

4. Conclusion

In this study, we successfully prepared PEI/NONOates-doped PLGA NPs (PLGA-PEI/NO NPs), examined their NO release and biofilm-binding ability, and evaluated anti-biofilm, antibacterial, and wound healing activities in MRSA biofilm-infected wounds in diabetic mice. PLGA-PEI/NO NPs have a sufficient NO loading along with a prolonged NO release over 4 days. PLGA-PEI/NO NPs effectively bound to the surface of the MRSA biofilm matrix, resulting in potent biofilm dispersal. Moreover, PLGA-PEI/NO NPs showed the complete removal of MRSA biofilms, the reduced wound bacterial burden, and the accelerated wound closure in MRSA biofilm-infected wounds in diabetic mice. Therefore, our novel biofilm-binding, NO-releasing NPs represent a promising NO delivery system for the treatments of biofilm-infected chronic wounds.

Acknowledgements

This research was supported by a grant from the Korean Healthcare Technology R&D Project, Ministry for Health and Welfare Affairs, Republic of Korea (HI15C2558).

Declarations of interest

None.

References

[1] G.A. James, E. Swogger, R. Wolcott, P. Secor, J. Sestrich, J.W. Costerton, P.S. Stewart, Biofilms in chronic wounds, Wound Repair and regeneration, 16 (2008) 37-44.

[2] A.I. Hochbaum, I. Kolodkin-Gal, L. Foulston, R. Kolter, J. Aizenberg, R. Losick, Inhibitory effects of D-amino acids on Staphylococcus aureus biofilm development, Journal of bacteriology, 193 (2011) 5616-5622.

[3] R. Yazdani, M. Oshaghi, A. Havayi, E. Pishva, R. Salehi, M. Sadeghizadeh, H. Foroohesh, Detection of icaAD gene and biofilm formation in Staphylococcus aureus isolates from wound infections, Iranian Journal of Public Health, 35 (2006) 25-28.

[4] K.A. Moran, C.K. Murray, E.L. Anderson, Bacteriology of blood, wound, and sputum cultures from non-US casualties treated in a combat support hospital in Iraq, Infection Control & Hospital Epidemiology, 29 (2008) 981-984.

[5] R.W. Care, A study of biofilm-based wound management in subjects with critical limb ischaemia, Journal of wound care, 17 (2008) 145.

[6] C.J. Sánchez, K. Mende, M.L. Beckius, K.S. Akers, D.R. Romano, J.C. Wenke, C.K. Murray, Biofilm formation by clinical isolates and the implications in chronic infections, BMC infectious diseases, 13 (2013) 47.

[7] D. Singhal, A. Foreman, J.J. Bardy, P.J. Wormald, Staphylococcus aureus biofilms, The Laryngoscope, 121 (2011) 1578-1583.

[8] J.-M.L. Iyamba, J.M. Wambale, C.M. Lukukula, High prevalence of methicillin resistant staphylococci strains isolated from surgical site infections in Kinshasa, The Pan African medical journal, 18 (2014).

[9] D.C. Kaur, S. Wankhede, Biofilm formation and antimicrobial susceptibility pattern of methicillin resistant Staphylococcus aureus from wound infection, Asian Pac J Health Sci, 1 (2014) 322-328.

[10] A. Belbase, N.D. Pant, K. Nepal, B. Neupane, R. Baidhya, R. Baidya, B. Lekhak, Antibiotic resistance and biofilm production among the strains of Staphylococcus aureus isolated from pus/wound swab samples in a tertiary care hospital in Nepal, Annals of clinical microbiology and antimicrobials, 16 (2017) 15.

[11] P. Neopane, H.P. Nepal, R. Shrestha, O. Uehara, Y. Abiko, In vitro biofilm formation by Staphylococcus aureus isolated from wounds of hospital-admitted patients and their association with antimicrobial resistance, International Journal of General Medicine, 11 (2018) 25.

[12] N. Parkhouse, P.M. Le Quesne, Impaired neurogenic vascular response in patients with diabetes and neuropathic foot lesions, New England Journal of Medicine, 318 (1988) 1306-1309.

[13] I. Uçkay, J. Aragón-Sánchez, D. Lew, B.A. Lipsky, Diabetic foot infections: what have we learned in the last 30 years?, International Journal of Infectious Diseases, 40 (2015) 81-91.

[14] M. Zubair, A. Malik, J. Ahmad, Incidence, risk factors for amputation among patients with diabetic foot ulcer in a North Indian tertiary care hospital, The Foot, 22 (2012) 24-30.

[15] D.D. Rhoads, R.D. Wolcott, S.L. Percival, Biofilms in wounds: management strategies, Journal of wound care, 17 (2008) 502-508.

[16] S.L. Percival, P. Kite, K. Eastwood, R. Murga, J. Carr, M.J. Arduino, R.M. Donlan, Tetrasodium EDTA as a novel central venous catheter lock solution against biofilm, Infection Control & Hospital Epidemiology, 26 (2005) 515-519.

[17] B.S. Atiyeh, M. Costagliola, S.N. Hayek, S.A. Dibo, Effect of silver on burn wound infection control and healing: review of the literature, burns, 33 (2007) 139-148.

[18] M.A. Fischbach, C.T. Walsh, Antibiotics for emerging pathogens, Science, 325 (2009) 1089-1093.

[19] G. Taubes, The bacteria fight back, in, American Association for the Advancement of Science, 2008.

[20] N. Barraud, M. J Kelso, S. A Rice, S. Kjelleberg, Nitric oxide: a key mediator of biofilm dispersal with applications in infectious diseases, Current pharmaceutical design, 21 (2015) 31-42.

[21] S.M. Deupree, M.H. Schoenfisch, Morphological analysis of the antimicrobial action of nitric oxide on Gram-negative pathogens using atomic force microscopy, Acta biomaterialia, 5 (2009) 1405-1415.
[22] J.-d. Luo, A.F. Chen, Nitric oxide: a newly discovered function on wound healing, Acta Pharmacologica Sinica, 26 (2005) 259.
[23] S.P. Hlaing, J. Kim, J. Lee, N. Hasan, J. Cao, M. Naeem, E.H. Lee, J.H. Shin, Y. Jung, B.-L. Lee, S-Nitrosoglutathione loaded poly (lactic-co-glycolic acid) microparticles for prolonged nitric oxide release and enhanced healing of methicillin-resistant Staphylococcus aureus-infected wounds, European Journal of Pharmaceutics and Biopharmaceutics, 132 (2018) 94-102.
[24] N. Barraud, D. Schleheck, J. Klebensberger, J.S. Webb, D.J. Hassett, S.A. Rice, S. Kjelleberg, Nitric oxide signaling in Pseudomonas aeruginosa biofilms mediates phosphodiesterase activity, decreased cyclic di-GMP levels, and enhanced dispersal, Journal of bacteriology, 191 (2009) 7333-7342.
[25] S. Schlag, C. Nerz, T.A. Birkenstock, F. Altenberend, F. Götz, Inhibition of staphylococcal biofilm formation by nitrite, Journal of bacteriology, 189 (2007) 7911-7919.
[26] L.R. Martinez, G. Han, M. Chacko, M.R. Mihu, M. Jacobson, P. Gialanella, A.J. Friedman, J.D. Nosanchuk, J.M. Friedman, Antimicrobial and healing efficacy of sustained release nitric oxide nanoparticles against Staphylococcus aureus skin infection, Journal of Investigative Dermatology, 129 (2009) 2463-2469.
[27] D.T. Efron, D. Most, A. Barbul, Role of nitric oxide in wound healing, Current Opinion in Clinical Nutrition & Metabolic Care, 3 (2000) 197-204.
[28] B.J. Nablo, A.R. Rothrock, M.H. Schoenfisch, Nitric oxide-releasing sol–gels as antibacterial coatings for orthopedic implants, Biomaterials, 26 (2005) 917-924.
[29] J.O. Kim, J.-K. Noh, R.K. Thapa, N. Hasan, M. Choi, J.H. Kim, J.-H. Lee, S.K. Ku, J.-W. Yoo, Nitric oxide-releasing chitosan film for enhanced antibacterial and in vivo wound-healing efficacy, International journal of biological macromolecules, 79 (2015) 217-225.
[30] X. Yao, Y. Liu, J. Gao, L. Yang, D. Mao, C. Stefanitsch, Y. Li, J. Zhang, L. Ou, D. Kong, Nitric oxide releasing hydrogel enhances the therapeutic efficacy of mesenchymal stem cells for myocardial infarction, Biomaterials, 60 (2015) 130-140.
[31] A.J. Friedman, G. Han, M.S. Navati, M. Chacko, L. Gunther, A. Alfieri, J.M. Friedman, Sustained release nitric oxide releasing nanoparticles: characterization of a novel delivery platform based on nitrite containing hydrogel/glass composites, Nitric Oxide, 19 (2008) 12-20.
[32] J.W. Yoo, J.S. Lee, C.H. Lee, Characterization of nitric oxide-releasing microparticles for the mucosal delivery, Journal of Biomedical Materials Research Part A, 92 (2010) 1233-1243.
[33] B. Sun, D.L. Slomberg, S.L. Chudasama, Y. Lu, M.H. Schoenfisch, Nitric oxide-releasing dendrimers as antibacterial agents, Biomacromolecules, 13 (2012) 3343-3354.
[34] Y.S. Jo, A.J. van der Vlies, J. Gantz, T.N. Thacher, S. Antonijevic, S. Cavadini, D. Demurtas, N. Stergiopulos, J.A. Hubbell, Micelles for delivery of nitric oxide, Journal of the American Chemical Society, 131 (2009) 14413-14418.
[35] G.M. Whitesides, Nanoscience, nanotechnology, and chemistry, Small, 1 (2005) 172-179.
[36] A.W. Carpenter, B.V. Worley, D.L. Slomberg, M.H. Schoenfisch, Dual action antimicrobials: nitric oxide release from quaternary ammonium-functionalized silica nanoparticles, Biomacromolecules, 13 (2012) 3334-3342.
[37] C. Macherla, D.A. Sanchez, M. Ahmadi, E.M. Vellozzi, A.J. Friedman, J.D. Nosanchuk, L.R. Martinez, Nitric oxide releasing nanoparticles for treatment of Candida albicans burn infections, Frontiers in microbiology, 3 (2012) 193.
[38] K.R. Raghupathi, R.T. Koodali, A.C. Manna, Size-dependent bacterial growth inhibition and mechanism of antibacterial activity of zinc oxide nanoparticles, Langmuir, 27 (2011) 4020-4028.
[39] N. Rajput, A. Bankar, Bio-inspired gold nanoparticles synthesis and their anti-biofilm efficacy, J. Pharm. Invest., 47 (2017) 521-530.

[40] C.H. Kim, S.G. Lee, M.J. Kang, S. Lee, Y.W. Choi, Surface modification of lipid-based nanocarriers for cancer cell-specific drug targeting, J. Pharm. Invest., 47 (2017) 203-227.
[41] H. Nurhasni, J. Cao, M. Choi, I. Kim, B.L. Lee, Y. Jung, J.-W. Yoo, Nitric oxide-releasing poly (lactic-co-glycolic acid)-polyethylenimine nanoparticles for prolonged nitric oxide release, antibacterial efficacy, and in vivo wound healing activity, Int. J. Nanomed., 10 (2015) 3065.
[42] J. Cao, J.-S. Choi, M. Oshi, J. Lee, H. Nurhasni, J. Kim, J.-W. Yoo, Development of PLGA micro-and nanorods with high capacity of surface ligand conjugation for enhanced targeted delivery, Asian Journal of Pharmaceutical Sciences, (2018).
[43] M. Naeem, J. Bae, M.A. Oshi, M.-S. Kim, H.R. Moon, B.L. Lee, E. Im, Y. Jung, J.-W. Yoo, Colon-targeted delivery of cyclosporine A using dual-functional Eudragit® FS30D/PLGA nanoparticles ameliorates murine experimental colitis, Int. J. Nanomed., 13 (2018) 1225.
[44] B.L. Furman, Streptozotocin-induced diabetic models in mice and rats, Current Protocols in Pharmacology, (2015) 5.47. 41-45.47. 20.
[45] K.M. Davies, D.A. Wink, J.E. Saavedra, L.K. Keefer, Chemistry of the diazeniumdiolates. 2. Kinetics and mechanism of dissociation to nitric oxide in aqueous solution, Journal of the American Chemical Society, 123 (2001) 5473-5481.
[46] G.-H. Son, B.-J. Lee, C.-W. Cho, Mechanisms of drug release from advanced drug formulations such as polymeric-based drug-delivery systems and lipid nanoparticles, J. Pharm. Invest., 47 (2017) 287-296.
[47] A.W. Smith, Biofilms and antibiotic therapy: is there a role for combating bacterial resistance by the use of novel drug delivery systems?, Advanced drug delivery reviews, 57 (2005) 1539-1550.
[48] G. Han, L.N. Nguyen, C. Macherla, Y. Chi, J.M. Friedman, J.D. Nosanchuk, L.R. Martinez, Nitric oxide–releasing nanoparticles accelerate wound healing by promoting fibroblast migration and collagen deposition, The American journal of pathology, 180 (2012) 1465-1473.
[49] H.-C. Flemming, J. Wingender, C. Mayer, V. Korstgens, W. Borchard, Cohesiveness in biofilm matrix polymers, in: Symposia-Society for General Microbiology, Cambridge; Cambridge University Press; 1999, 2000, pp. 87-106.
[50] M. Maifreni, F. Frigo, I. Bartolomeoli, S. Buiatti, S. Picon, M. Marino, Bacterial biofilm as a possible source of contamination in the microbrewery environment, Food Control, 50 (2015) 809-814.
[51] T. Wong, J. McGrath, H. Navsaria, The role of fibroblasts in tissue engineering and regeneration, British Journal of Dermatology, 156 (2007) 1149-1155.
[52] H. Yanagida, M. Okada, M. Masuda, M. Ueki, I. Narama, S. Kitao, Y. Koyama, T. Furuzono, K. Takakuda, Cell adhesion and tissue response to hydroxyapatite nanocrystal-coated poly (L-lactic acid) fabric, Journal of bioscience and bioengineering, 108 (2009) 235-243.
[53] E.M. Hetrick, J.H. Shin, H.S. Paul, M.H. Schoenfisch, Anti-biofilm efficacy of nitric oxide-releasing silica nanoparticles, Biomaterials, 30 (2009) 2782-2789.
[54] A.K. Balin, L. Pratt, Dilute povidone-iodine solutions inhibit human skin fibroblast growth, Dermatologic surgery, 28 (2002) 210-214.
[55] H.C. Pyo, Y.K. Kim, K.U. Whang, Y.L. Park, H.C. Eun, A comparative study of cytotoxicity of topical antimicrobials to cultured human keratinocytes and fibroblasts, Korean Journal of Dermatology, 33 (1995) 895-906.
[56] R.J. White, K. Cutting, A. Kingsley, Topical antimicrobials in the control of wound bioburden, Ostomy/wound management, 52 (2006) 26-58.
[57] C.J. Backlund, B.V. Worley, M.H. Schoenfisch, Anti-biofilm action of nitric oxide-releasing alkyl-modified poly (amidoamine) dendrimers against Streptococcus mutans, Acta biomaterialia, 29 (2016) 198-205.
[58] Y. Lu, D.L. Slomberg, A. Shah, M.H. Schoenfisch, Nitric oxide-releasing amphiphilic poly (amidoamine)(PAMAM) dendrimers as antibacterial agents, Biomacromolecules, 14 (2013) 3589-3598.

[59] H. Jin, L. Yang, M.J.R. Ahonen, M.H. Schoenfisch, Nitric Oxide-Releasing Cyclodextrins, Journal of the American Chemical Society, 140 (2018) 14178-14184.
[60] N.B. Menke, K.R. Ward, T.M. Witten, D.G. Bonchev, R.F. Diegelmann, Impaired wound healing, Clinics in dermatology, 25 (2007) 19-25.
[61] M. Schäffer, P.A. Efron, F.J. Thornton, K. Klingel, S.S. Gross, A. Barbul, Nitric oxide, an autocrine regulator of wound fibroblast synthetic function, The Journal of Immunology, 158 (1997) 2375-2381.

Figure Captions

Fig. 1. Schematic illustration of preparation of PLGA-PEI/NO NPs.

Fig. 2. Characterization of NPs. (a) SEM images of PLGA-PEI NPs and PLGA-PEI/NO NPs; bars represent 500 nm. (b) Size distribution of PLGA-PEI NPs and PLGA-PEI/NO NPs by qNano analysis; insets represent zeta potential measurement by Malvern Zetasizer. (c) *In vitro* release profile of PLGA-PEI/NO NPs. All samples were placed in SWF at 37 °c; data are presented as the mean ± SD; n=4.

Fig. 3. Adhesion of NPs to the biofilm matrix. (a) 2D images showed biofilm EPS (red) stained with tritc and NPs (green) stained with coumarin-6. All samples were incubated for 2 h. (b) Schematic presentation of NP binding to the biofilm matrix.

Fig. 4. *In vitro* anti-biofilm activity of PLGA-PEI/NO NPs. MRSA biofilms were grown on coupon for up to 24 h in the presence or absence of PLGA-PEI NPs or PLGA-PEI/NO NPs. (a) Crystal violet-stained biofilms on coupon; deep blue color indicates biofilm and yellow color indicates biofilm dispersal. enlarged confocal microscopy images showed live bacteria stained with SYTO-9 (green color) and dead bacteria stained with PI (red color). (b) Biofilm biomass determined by crystal violet staining (OD_{550}). values, mean ± sd; replicates, n=6; *P<0.05, compared to untreated group.

Fig. 5. Viability (%) of L929 mouse fibroblast cells after 24 h exposure to PLGA NPs, PLGA-PEI NPs, and PLGA-PEI/NO NPs at various concentration (n = 8).

Fig. 6. Biofilm-infected wounds in STZ-induced diabetic ICR mice. (a) Representative photographs of healing in STZ-induced diabetic ICR mice with MRSA biofilm challenge treated with or without PLGA-PEI/NO NPs. (b) Wound area reduction percentage of mice skin lesions relative to the initial 8-mm wound. data shown are mean ± SD; n=10, different wounds; *P<0.05, compared with untreated group. (c) Wound closure percentage of mice skin lesions at last day relative to the initial 8-mm wound.

Fig. 7. Histological analysis (H&E and Masson's trichrome stain) of MRSA biofilm-infected wounds in STZ-induced diabetic ICR mice at last day. Scale bar = 50 μm; EP = epidermal; DE = dermal junction; HD = hypodermis; G = granulation tissue; M = wound matrix. Orange arrows indicate early epithelialization, red arrows indicate fibroblast cells, and black arrows

denote mononuclear inflammatory cells. Blue color in trichrome stained images indicates collagen arranged in parallel to the surface.

Fig. 8. Bacterial burden in the wound. (a) Viability of bacteria in the wound determined using the CFU method. (b) Gram staining of the skin tissue. Purple color spots marked with arrows represent MRSA colonies. At day 2, 8, and 12 after biofilm infection, wounds were swabbed and the bacterial burden was examined. (c) 3D *in vivo* biofilm dispersal in biopsy samples collected on day 0 and on treatment days 4, 6, 8, and 10, analyzed by confocal microscopy (side view images).

Fig. 1.

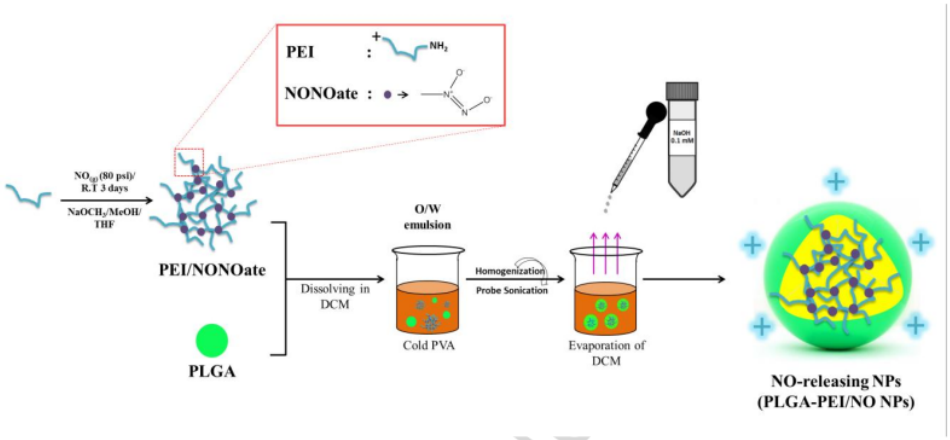

Fig. 2.

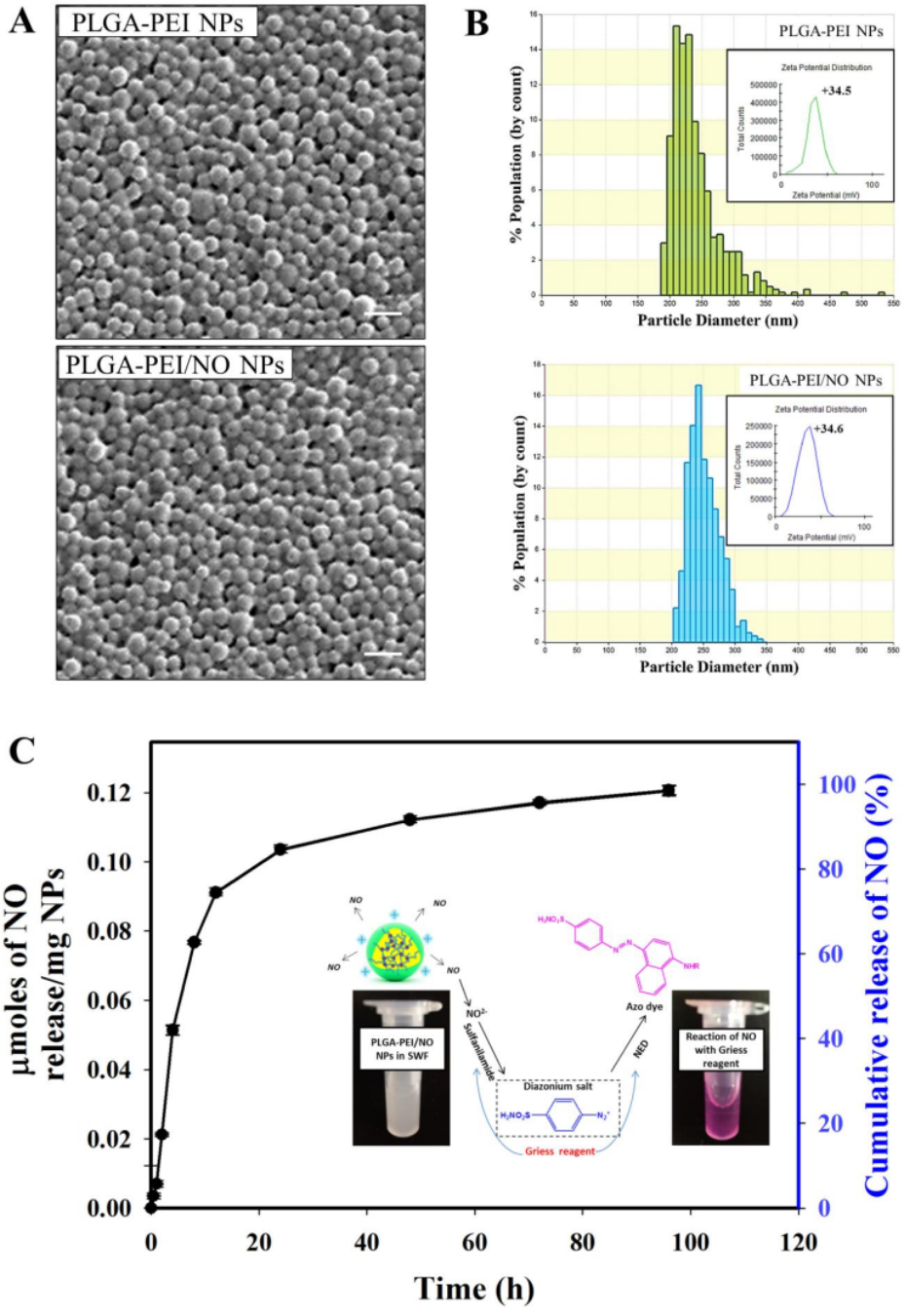

Fig. 3.

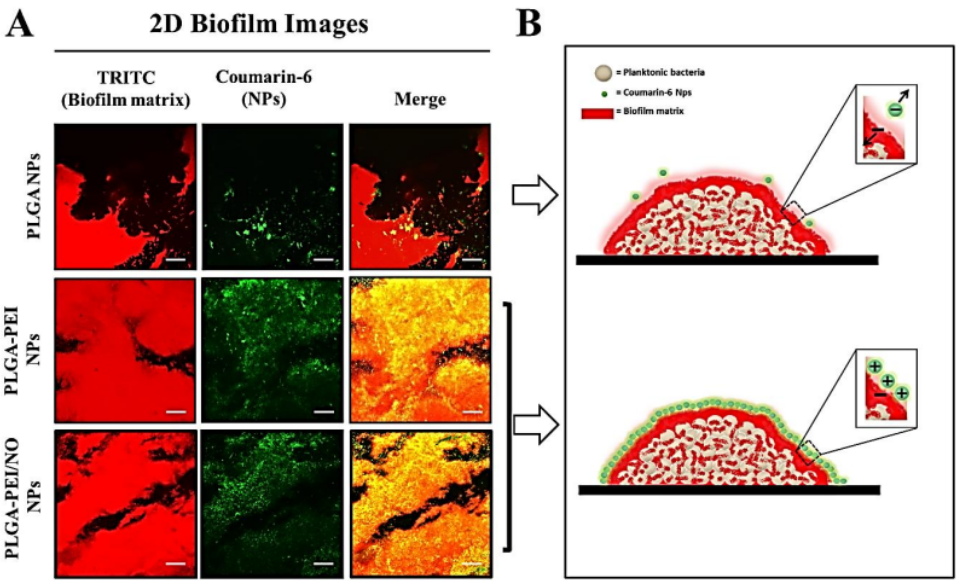

Fig. 4.

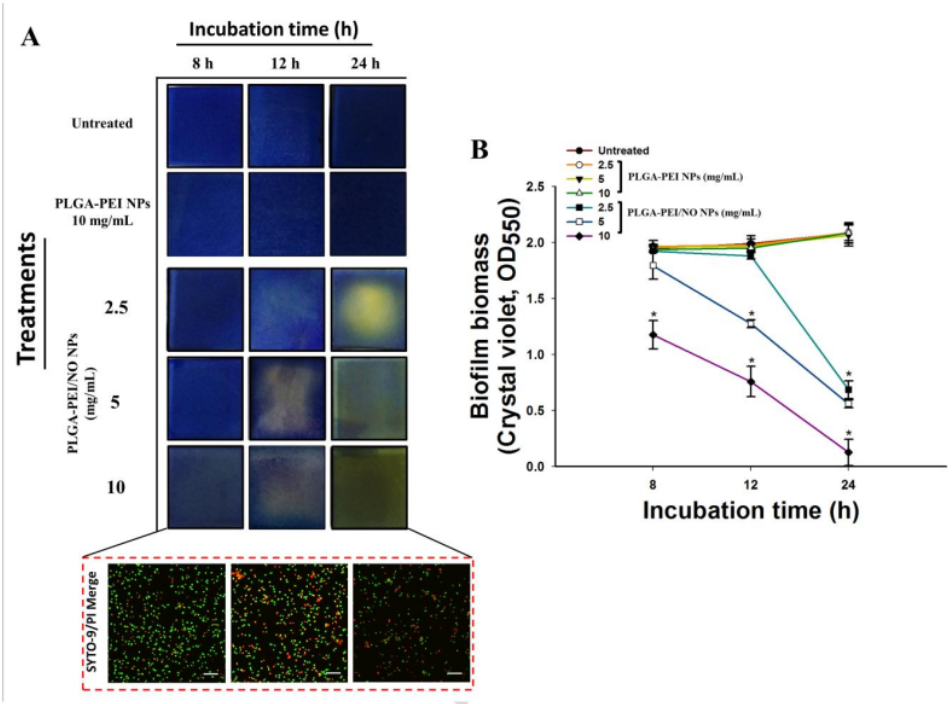

Fig. 5.

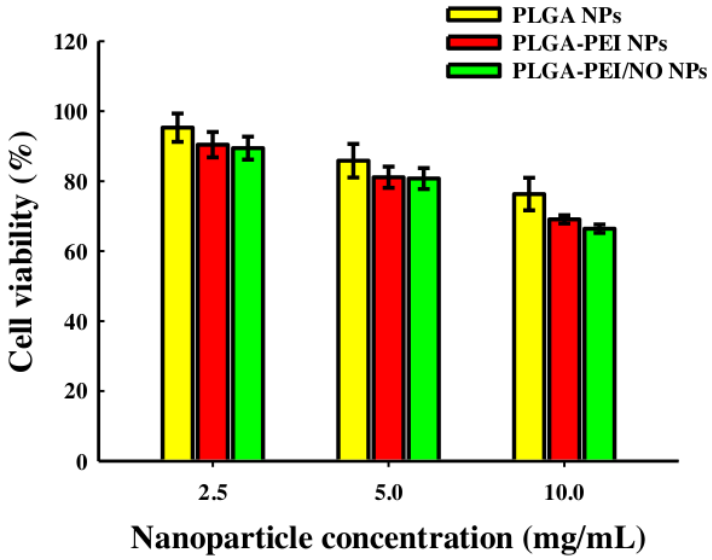

Fig. 6.

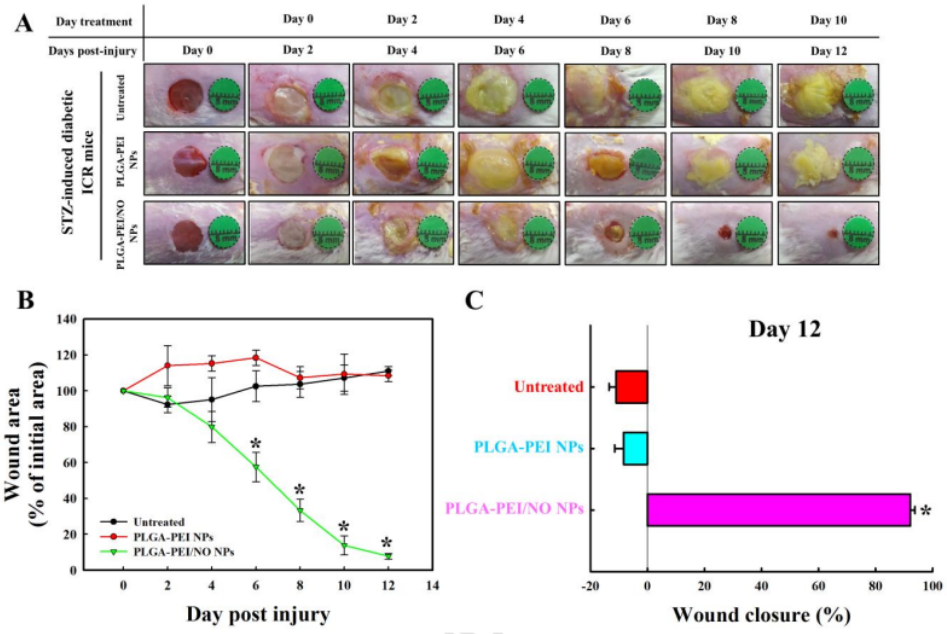

Fig. 7.

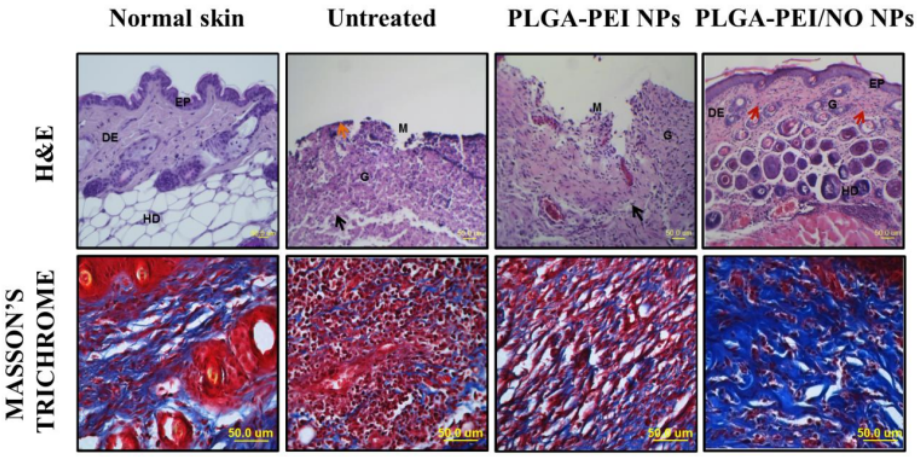

Fig. 8.

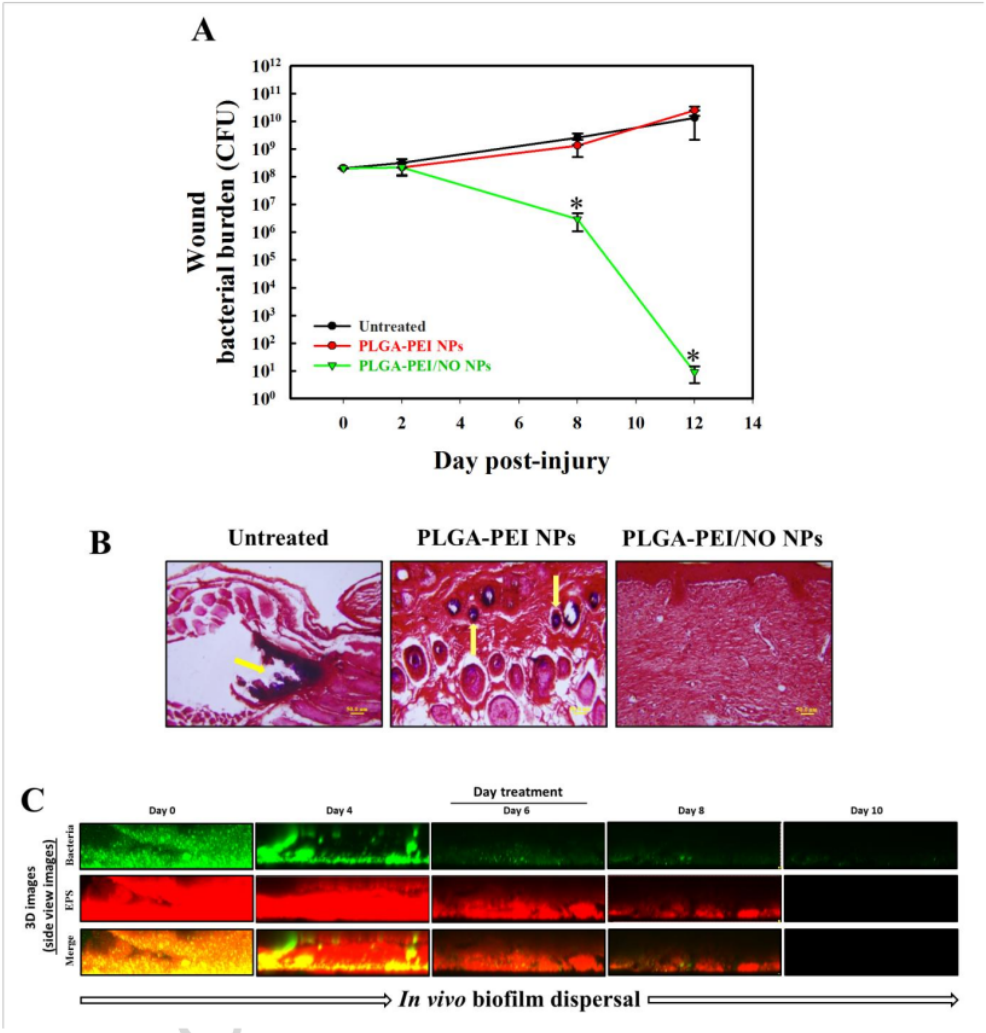

Table 1. Characterization of NPs

NPs	Amount of loaded NO (µmoles/g NPs)	Size (nm)		PDI	Zeta Potential (mV)
		Zetasizer	qNano		
PLGA NPs	N.D	252 ± 45	246 ± 49	0.133	- 24.3 ± 1.7
PLGA-PEI NPs	N.D	265 ± 11	248 ± 46	0.091	+ 34.5 ± 1.2
PLGA-PEI/NO NPs	122 ± 1	240 ± 2	247 ± 26	0.080	+ 34.6 ± 1.1

Values are expressed as mean ± SD of three different batches of particles

Highlights

- Nitric oxide has been successfully incorporated into the polymeric nanoparticles (PLGA-PE/NO NPs).
- PLGA-PEI/NO NPs effectively bind to the surface of the biofilm matrix, causing strong biofilm dispersal *in vitro* and *in vivo*.
- PLGA-PEI/NO NPs can effectively treat biofilm-infected wound in diabetic mice model by clearing the infection and promoting wound healing.
- The novel biofilm-binding, NO-releasing NPs represent a promising technology for the development of high-efficacy treatments for biofilm-infected chronic wounds.

12th_Paper_Nurhasni_Hasan_(2019).pdf

ORIGINALITY REPORT

23%	16%	19%	4%
SIMILARITY INDEX	INTERNET SOURCES	PUBLICATIONS	STUDENT PAPERS

PRIMARY SOURCES

1	Submitted to Yeungnam University Student Paper	1%
2	Chi Juan Ma, Yunfan He, Xiaoxuan Jin, Yuchen Zhang, Xiangdong Zhang, Yibao Li, Mimi Xu, Kaiyang Liu, Yao Yao, Feng Lu. "Light-regulated nitric oxide release from hydrogel-forming microneedles integrated with graphene oxide for biofilm-infected-wound healing", Materials Science and Engineering: C, 2021 Publication	1%
3	pubs.rsc.org Internet Source	1%
4	Blecher, Karin, Luis R. Martinez, Chaim Tuckman-Vernon, Parimala Nacharaju, David Schairer, Jason Chouake, Joel M. Friedman, Alan Alfieri, Chandan Guha, Joshua D. Nosanchuk, and Adam J. Friedman. "Nitric oxide-releasing nanoparticles accelerate wound healing in NOD-SCID mice",	1%

Nanomedicine Nanotechnology Biology and Medicine, 2012.
Publication

5	test.dovepress.com Internet Source	1 %
6	Jisong Hua, Peng Teng, Yingying Zou, Chao Zhang, Xujie Shen, Jianfeng Cai, Yong Hu. "Small antimicrobial agents encapsulated in poly(epsilon-caprolactone)-poly(ethylene glycol) nanoparticles for treatment of S. aureus-infected wounds", Journal of Nanoparticle Research, 2018 Publication	1 %
7	Mahmoud Nasrollahzadeh, Fahimeh Soleimani, Nayyereh Sadat Soheili Bidgoli, Nasrin Shafiei, Zahra Nezafat, Talat Baran. "Biological applications of biopolymer-based (nano)materials", Elsevier BV, 2021 Publication	1 %
8	unsworks.unsw.edu.au Internet Source	1 %
9	www.omicsonline.org Internet Source	1 %
10	coek.info Internet Source	1 %
11	HaeYong Seok, Jin Yong Noh, Dae Yong Lee, Sung Jin Kim, Chang Seon Song, Yeu Chun	<1 %

Kim. "Effective humoral immune response from a H1N1 DNA vaccine delivered to the skin by microneedles coated with PLGA-based cationic nanoparticles", Journal of Controlled Release, 2017
Publication

12	Nikita Sharma, R. Mankamna Kumari, Nidhi Gupta, Asad Syed, Ali H. Bahkali, Surendra Nimesh. "Poly-(Lactic-co-Glycolic) Acid Nanoparticles for Synergistic Delivery of Epirubicin and Paclitaxel to Human Lung Cancer Cells", Molecules, 2020 Publication	<1 %
13	hdl.handle.net Internet Source	<1 %
14	etheses.whiterose.ac.uk Internet Source	<1 %
15	Luis R Martinez. "Antimicrobial and Healing Efficacy of Sustained Release Nitric Oxide Nanoparticles Against Staphylococcus Aureus Skin Infection", Journal of Investigative Dermatology, 04/23/2009 Publication	<1 %
16	www.dovepress.com Internet Source	<1 %
17	www.annlabmed.org Internet Source	<1 %

18	www.frontiersin.org Internet Source	<1 %
19	Submitted to National Chung Hsing University Student Paper	<1 %
20	Submitted to University of Sheffield Student Paper	<1 %
21	Ramesh Duwa, Asmita Banstola, Fakhrossadat Emami, Jee-Heon Jeong, Sooyeun Lee, Simmyung Yook. "Cetuximab conjugated temozolomide-loaded poly (lactic-co-glycolic acid) nanoparticles for targeted nanomedicine in EGFR overexpressing cancer cells", Journal of Drug Delivery Science and Technology, 2020 Publication	<1 %
22	George Han. "Nitric Oxide Releasing Nanoparticles Are Therapeutic for Staphylococcus aureus Abscesses in a Murine Model of Infection", PLoS ONE, 11/12/2009 Publication	<1 %
23	cdr.lib.unc.edu Internet Source	<1 %
24	worldwidescience.org Internet Source	<1 %
25	www.nature.com Internet Source	<1 %

26	Yujie Ji, Guowei Li, Wu Zhang, Dong Ma, Wei Xue. "Cross-linked branched polyethylenimine used as a nitric oxide donor for prolonged nitric oxide release", Materials Science and Engineering: C, 2017 Publication	<1 %
27	link.springer.com Internet Source	<1 %
28	Yash S. Raval, Abdelrhman Mohamed, Jayawant N. Mandrekar, Cody Fisher et al. " Anti-Biofilm Activity of Hydrogen-Peroxide Generating Electrochemical Bandage Against Yeast Biofilms ", Antimicrobial Agents and Chemotherapy, 2021 Publication	<1 %
29	pdfs.semanticscholar.org Internet Source	<1 %
30	Submitted to University of Sydney Student Paper	<1 %
31	lan.sagepub.com Internet Source	<1 %
32	tohoku.repo.nii.ac.jp Internet Source	<1 %
33	Anthony Ku, Conrad Chan, Sadaf Aghevlian, Zhongli Cai et al. " MicroSPECT/CT Imaging of Cell-Line and Patient-Derived EGFR-Positive	<1 %

	Tumor Xenografts in Mice with Panitumumab Fab Modified with Hexahistidine Peptides To Enable Labeling with Tc(I) Tricarbonyl Complex ", Molecular Pharmaceutics, 2019 Publication	
34	diposit.ub.edu Internet Source	<1 %
35	academic.oup.com Internet Source	<1 %
36	topsecretapiaccess.dovepress.com Internet Source	<1 %
37	Rachna N. Dave, Hiren M. Joshi, Vayalam P. Venugopalan. "Biomedical evaluation of a novel nitrogen oxides releasing wound dressing", Journal of Materials Science: Materials in Medicine, 2012 Publication	<1 %
38	Wan-Uk Kim, Woo-Kyoung Lee, Jae-Woong Ryoo, Seung-Hoon Kim et al. "Suppression of collagen-induced arthritis by single administration of poly(lactic-co-glycolic acid) nanoparticles entrapping type II collagen: A novel treatment strategy for induction of oral tolerance", Arthritis & Rheumatism, 2002 Publication	<1 %
39	journals.sagepub.com Internet Source	<1 %

40	Ann Schwentker, Yoram Vodovotz, Richard Weller, Timothy R Billiar. "Nitric oxide and wound repair: role of cytokines?", Nitric Oxide, 2002 Publication	<1 %
41	Ji Young Lee, Byung Pal Yu, Hae Young Chung. " Activation mechanisms of endothelial NF-κB, IKK, and MAP kinase by -butyl hydroperoxide ", Free Radical Research, 2009 Publication	<1 %
42	Jing Li, Jun Zhang, Yiyue Wang, Xiao Liang, Zaitongguli Wusiman, Yunzhi Yin, Qi Shen. "Synergistic inhibition of migration and invasion of breast cancer cells by dual docetaxel/quercetin-loaded nanoparticles via Akt/MMP-9 pathway", International Journal of Pharmaceutics, 2017 Publication	<1 %
43	Submitted to University of Hong Kong Student Paper	<1 %
44	digitalcommons.library.tmc.edu Internet Source	<1 %
45	eprints.soton.ac.uk Internet Source	<1 %
46	lib.dr.iastate.edu Internet Source	<1 %

47	synapse.koreamed.org Internet Source	<1 %
48	Jain, Rishabh, Ankit Agarwal, Patricia R. Kierski, Michael J. Schurr, Christopher J. Murphy, Jonathan F. McAnulty, and Nicholas L. Abbott. "The use of native chemical functional groups presented by wound beds for the covalent attachment of polymeric microcarriers of bioactive factors", Biomaterials, 2013. Publication	<1 %
49	Ke Xu, Ningchen An, Haijuan Zhang, Qilu Zhang et al. "Sustained-release of PDGF from PLGA microsphere embedded thermo-sensitive hydrogel promoting wound healing by inhibiting autophagy", Journal of Drug Delivery Science and Technology, 2020 Publication	<1 %
50	Meital Ben David-Naim, Etty Grad, Gil Aizik, Mirjam M. Nordling-David, Ofra Moshel, Zvi Granot, Gershon Golomb. "Polymeric nanoparticles of siRNA prepared by a double-emulsion solvent-diffusion technique: Physicochemical properties, toxicity, biodistribution and efficacy in a mammary carcinoma mice model", Biomaterials, 2017 Publication	<1 %
51	Na Wang, Huanghuang Xu, Shian Sun, Pengyue Guo, Yuan Wang, Chuntong Qian,	<1 %

Yuanyuan Zhong, Dongzhi Yang. "Wound therapy via a photo-responsively antibacterial nano-graphene quantum dots conjugate", Journal of Photochemistry and Photobiology B: Biology, 2020
Publication

52	Yan Nie, Kaiyue Zhang, Shuaiqiang Zhang, Dan Wang et al. "Nitric oxide releasing hydrogel promotes endothelial differentiation of mouse embryonic stem cells", Acta Biomaterialia, 2017 Publication	<1 %
53	Zaid Muwaffak, Alvaro Goyanes, Vivienne Clark, Abdul W. Basit, Stephen T. Hilton, Simon Gaisford. "Patient-specific 3D scanned and 3D printed antimicrobial polycaprolactone wound dressings", International Journal of Pharmaceutics, 2017 Publication	<1 %
54	bmccomplementmedtherapies.biomedcentral.com Internet Source	<1 %
55	core.ac.uk Internet Source	<1 %
56	ir.library.osaka-u.ac.jp Internet Source	<1 %
57	journal.frontiersin.org Internet Source	<1 %

58	journals.lww.com Internet Source	<1 %
59	kjim.org Internet Source	<1 %
60	www.doria.fi Internet Source	<1 %
61	www.fedoa.unina.it Internet Source	<1 %
62	www.researchgate.net Internet Source	<1 %
63	"Abstracts", Joint Bone Spine, 200603 Publication	<1 %
64	Badia Douhri, Khalid Draoui, Ihssane Raissouni, Mohamed Hadri et al. "Chemical composition and biological activity of essential oil of the Moroccan endemic Origanum grosii", Materials Today: Proceedings, 2023 Publication	<1 %
65	Ghaffari, A.. "Potential application of gaseous nitric oxide as a topical antimicrobial agent", Nitric Oxide, 200602 Publication	<1 %
66	J. Rosen, A. Landriscina, J.D. Nosanchuk. "Nitric Oxide–Releasing Nanoparticles as an Antimicrobial Therapeutic", Elsevier BV, 2016	<1 %

	Publication	
67	Parani, Madasamy, Giriraj Lokhande, Ankur Singh, and Akhilesh K Gaharwar. "Engineered Nanomaterials for Infection Control and Healing Acute and Chronic Wounds", ACS Applied Materials & Interfaces Publication	<1 %
68	Silva, R.. "Protein microspheres as suitable devices for piroxicam release", Colloids and Surfaces B: Biointerfaces, 20120401 Publication	<1 %
69	Weijun Xiu, Ling Wan, Kaili Yang, Xiao Li, Lihui Yuwen, Heng Dong, Yongbin Mou, Dongliang Yang, Lianhui Wang. "Potentiating hypoxic microenvironment for antibiotic activation by photodynamic therapy to combat bacterial biofilm infections", Nature Communications, 2022 Publication	<1 %
70	clok.uclan.ac.uk Internet Source	<1 %
71	doi.org Internet Source	<1 %
72	doria.fi Internet Source	<1 %
73	orca.cardiff.ac.uk Internet Source	<1 %

74	os.zhdk.cloud.switch.ch Internet Source	<1 %
75	pure.ulster.ac.uk Internet Source	<1 %
76	scholarbank.nus.edu.sg Internet Source	<1 %
77	www.arxiv-vanity.com Internet Source	<1 %
78	www.eurasianbiochem.org Internet Source	<1 %
79	www.hindawi.com Internet Source	<1 %
80	www.tandfonline.com Internet Source	<1 %
81	Chae Young Kim, Bobin Kang, Hyung Joo Suh, Hyeon-Son Choi. "Red ginseng-derived saponin fraction suppresses the obesity-induced inflammatory responses via Nrf2-HO-1 pathway in adipocyte-macrophage co-culture system", Biomedicine & Pharmacotherapy, 2018 Publication	<1 %
82	Mei Yang, Lingling Sheng, Tian R. Zhang, Qingfeng Li. "Stem Cell Therapy for Lower Extremity Diabetic Ulcers: Where Do We Stand?", BioMed Research International, 2013	<1 %

Publication

83	Muhammad Naeem, Wooseong Kim, Jiafu Cao, Yunjin Jung, Jin-Wook Yoo. "Enzyme/pH dual sensitive polymeric nanoparticles for targeted drug delivery to the inflamed colon", Colloids and Surfaces B: Biointerfaces, 2014 Publication	<1 %
84	Ju-Hwan Park, Hyun-Jong Cho, Dae-Duk Kim. "Poly((D,L)lactic-glycolic)acid–star glucose nanoparticles for glucose transporter and hypoglycemia-mediated tumor targeting", International Journal of Nanomedicine, 2017 Publication	<1 %

Exclude quotes	On	Exclude matches	< 5 words
Exclude bibliography	On		